RESEARCH ARTICLE
SPACE PHYSICS: MAGNETOSPHERIC PHYSICS

Earth and Planetary Physics
9: 148–158, 2025
doi: 10.26464/epp2025008

An embedded electron current layer observed at the edge of the plasma sheet in the Earth's magnetotail

ChenChen Zhan[1,2,3], RongSheng Wang[1,2,3*], QuanMing Lu[1,2,3], San Lu[1,2,3], and XinMin Li[1,2,3]

[1]Deep Space Exploration Laboratory/School of Earth and Space Sciences, University of Science and Technology of China, Hefei 230026, China;

[2]Chinese Academy of Sciences (CAS) Center for Excellence in Comparative Planetology/CAS Key Laboratory of Geospace Environment/Anhui Mengcheng National Geophysical Observatory, University of Science and Technology of China, Hefei 230026, China;

[3]Collaborative Innovation Center of Astronautical Science and Technology, Harbin 150001, China

Key Points:

- We report a sub-ion-scale electron current layer embedded at the edge of the plasma sheet in the Earth's magnetotail.
- The $\boldsymbol{E} \times \boldsymbol{B}$ drift of electrons gives rise to this current layer.
- The current layer has no magnetic reconnection signatures, and magnetic reconnection could be suppressed inside this layer.

Citation: Zhan, C. C., Wang, R. S., Lu, Q. M., Lu, S., and Li, X. M. (2025). An embedded electron current layer observed at the edge of the plasma sheet in the Earth's magnetotail. *Earth Planet. Phys.*, *9*(1), 148–158. http://doi.org/10.26464/epp2025008

Abstract: The formation of an embedded electron current sheet within the magnetotail plasma sheet has been poorly understood. In this article, we present an electron current layer detected at the edge of the magnetotail plasma sheet. The ions were demagnetized inside the electron current layer, but the electrons were still frozen in with the magnetic field line. Thus, this decoupling of ions and electrons gave rise to a strong Hall electric field, which could be the reason for the formation of the embedded thin current layer. The magnetized electrons, the absence of the nongyrotropic electron distribution, and negligible energy dissipation in the layer indicate that magnetic reconnection had not been triggered within the embedded thin current layer. The highly asymmetric plasma on the two sides of the current layer and low magnetic shear across it could suppress magnetic reconnection. The observations indicate that the embedded electric current layer, probably generated by the Hall electric field, even down to electron scale, is not a sufficient condition for magnetic reconnection.

Keywords: magnetotail; plasma sheet; magnetic reconnection

1. Introduction

The current sheet in the Earth's magnetotail plays a vital role in the storage of energy and mass from the solar wind to the near-Earth space (Ness, 1965; Russell and McPherron, 1973; Baker et al., 1996; Baumjohann, 2002). The stored magnetic energy will eventually be released at the time when certain kinds of instabilities (e.g., magnetic reconnection or current disruption) occur within the current sheet. As a result, a substorm will be triggered, resulting in a strong global magnetic field disturbance and particle injection into the magnetosphere and ionosphere. Substantial efforts have been devoted to investigating the magnetotail current sheet and its role in the process of generating magnetospheric substorms (Asano et al., 2003, 2004; Nakamura et al., 2006; Shen C et al., 2008a; Wang RS et al., 2018, 2020; Sitnov et al., 2019; Lu S et al., 2020; Genestreti et al., 2023). To simplify, the Harris current sheet model (Harris, 1962) was previously widely used to denote the magnetotail current sheet. However, the observed current profile across the magnetotail by *in situ* measurement usually deviated from the Harris model.

Multipoint simultaneous observations have indicated that the configuration and structure of the magnetotail current sheet is complicated and dynamic, with flapping, tilting, bifurcation, twisting, embedding, and so on (Zhang TL et al., 2002; Runov et al., 2003, 2005, 2006; Sergeev et al., 2003, 2004; Asano et al., 2005; Baumjohann et al., 2007; Shen C et al., 2008b). The magnetotail current sheet generally displays a multilayer structure, in which a thin electron current sheet is embedded inside a much broader plasma sheet (e.g., Petrukovich et al., 2011). This thin current sheet is ion scale or sub-ion scale, and the current within it is primarily carried by electrons. Previous studies have revealed some possible mechanisms for current sheet formation, such as the tearing mode instability, the Kelvin–Helmholtz instability, or the evolution of turbulence (Zhong ZH et al., 2018; Zhou M et al., 2019a, 2021). Although the configuration and formation of the current sheet have been studied extensively, it is still unclear how this thin current sheet is generated.

In this article, we report a sub-ion-scale electron current layer at

First author: C. C. Zhan, zcc18051103@mail.ustc.edu.cn
Correspondence to: R. S. Wang, rswan@ustc.edu.cn
Received 31 JUL 2024; Accepted 26 NOV 2024.
First Published online 17 DEC 2024.

the edge of the plasma sheet in the Earth's magnetotail. This current layer was formed by the Hall electric field drift of electrons. The magnetized electrons, the absence of the nongyrotropic electron distribution, and negligible energy dissipation indicated no magnetic reconnection signatures within the current layer. The reason for no magnetic reconnection in the electron current layer is addressed.

2. Observations

The Magnetospheric Multiscale (MMS) mission (Burch et al., 2016) consists of four satellites equipped with identical instruments, including a magnetometer (Russell et al., 2016), electric field instruments (Ergun et al., 2016; Lindqvist et al., 2016), and Fast Plasma Investigation (FPI) instruments (Pollock et al., 2016). The magnetic field is sampled at 128 samples/s, and the electric field is sampled at 8192 samples/s in burst mode. The time resolutions for electrons and ions taken from the FPI in burst mode are 30 and 150 ms, respectively, and their energy range is ~10 eV–30 keV. High-energy ion flux (~60–560 keV) is measured by the Fly's Eye Energetic Particle Spectrometer (FEEPS; Blake et al., 2016). Proton data from the Hot Plasma Composition Analyzer (HPCA; Young et al., 2016), with an energy range of ~10 eV–40 keV and a 10 s resolution, and from the Energetic Ion Spectrometer (EIS; Mauk et al., 2016), which has an energy range of 45–500 keV and a 20 s resolution, are also shown for comparison with ion data from the FPI. The separation of the four satellites was less than 20 km in the event studied here, and the observations at the four satellites displayed no obvious distinction. To remove the high-frequency noise, the data in the barycenter was used in this work unless otherwise stated. The electron bulk flow velocity $\boldsymbol{v}_{\mathrm{e}}$ in the barycenter was averaged again, with a sliding window of 0.06 s in particular, to further reduce noise.

2.1 An Asymmetric Current Layer Embedded at the Edge of the Plasma Sheet

From 12:04:55 to 12:06:20 universal time (UT) on August 4, 2017, the MMS was located at [−20.7, 5.5, 5.8] R_{E} in the Geocentric Solar Ecliptic (GSE) coordinate system and passed through the magnetotail plasma sheet. Figure 1 shows an overview of this crossing event. During the interval, B_X varied from ~22.8 nT at 12:05:07 UT to ~−10 nT at 12:06:10 UT, which indicates that the MMS spacecraft crossed the plasma sheet from the northern hemisphere to the southern hemisphere (Figure 1b). Magnetic field B_X was equal to 0 at 12:05:43.51 UT (the vertical dashed line), meaning the MMS reached the neutral sheet at that time. The ion (Figure 1g) and electron (Figure 1h) temperatures peaked locally around the neutral sheet. The plasma β (Figure 1a) was larger than 3 during the entire crossing, which indicates that the spacecraft was inside the plasma sheet of the magnetotail. According to previous observations (e.g., Wang RS et al., 2018, 2020), the plasma density and temperature peaked at the neutral sheet, and the magnetic field magnitude had the minimum value. However, the density (Figure 1a) and magnetic field strength (black trace in Figure 1b) were nearly constant around the neutral sheet in this event. Furthermore, around the neutral sheet, the ion (Figure 1d) and electron (Figure 1e) bulk flows were nearly constant and mainly directed duskward, and the current density (Figure 1f) was more or less equal to the background value without the expected peak. All these features suggest that the plasma sheet severely deviated from the normal observations of the magnetotail plasma sheet.

In the crossing of the plasma sheet, the ion bulk flow was enhanced mainly in the northern hemisphere from 12:05:00 to 12:05:40 UT. Ion velocities v_{iY} and v_{iZ} were positive and peaked (>100 km/s) at ~12:05:23 UT, whereas v_{iX} was negative and weak (<100 km/s). The electron bulk flow showed a similar evolution but increased significantly from 12:05:24 to 12:05:29.4 UT (up to 700 km/s; Figure 1e), as marked by the vertical dotted lines in Figure 1. This short enhancement of the electron bulk flow corresponded to the rise of the current density (i.e., the encounter of an embedded current layer; Figure 1f), which is labeled by the two vertical dotted lines (at 12:05:25.0 and 12:05:29.4 UT) in Figure 1. Within the current layer, $J_{\|}$ was negative up to −70 nA/m^2, which came basically from positive v_{eX} (i.e., the earthward transport of electrons; Figure 1e). In addition to the field-aligned component, the positive v_{eY} and v_{eZ} resulted in the formation of the intense perpendicular current component $J_{\perp}$, and its magnitude was up to 60 nA/m^2, comparable to that of the field-aligned component.

Before the encounter of the current layer, the plasma density and β were relatively low and the magnetic field strength was nearly constant (~23 nT). Within the current layer, the magnetic field evolved rapidly. The B_X and $|B|$ gradually declined, the B_Z and B_Y began to rise, and the plasma number density (black curve in Figure 1a) and the plasma β (red curve in Figure 1a) began to grow quickly. Thus, the gradients of the plasma density and the magnetic field strength were strong across the current layer. After the current layer, the plasma density and plasma β remained at a high level, and the magnetic field magnitude became constant again (~13 nT). The average number density was ~0.6 cm^{-3} above the layer and became ~0.7 cm^{-3} below the layer, whereas the plasma β was ~4 above the layer and was ~25 below the layer. In other words, the plasma parameters on both sides above (prior to 12:05:25 UT) and below (after 12:05:30 UT) the current layer were clearly asymmetric and a strong gradient of the magnetic field existed in the current layer. The plasma asymmetry could also be found in the ion and electron temperatures (Figures 1g and 1h) across the current layer. Furthermore, a strong electric field could be observed throughout the entire interval when the MMS was in the northern hemisphere (Figure 1c). The E_Y and E_Z gradually increased as the MMS approached the thin current layer ($|B|$ decreased slowly; Figure 1b) and sharply enhanced to more than 15 mV/m in the current layer (Figure 1c).

Figure 2 shows the ion data from multiple instruments with different energy ranges. The total pressure after the current layer crossing was higher than that before the crossing (i.e., the pressure was unbalanced across the current layer; Figure 2d). The unbalanced pressure was mainly contributed by sharp variation in the plasma pressure, which was basically attributed to the ion thermal pressure measured from the FPI. The ion energy spectrogram (Figure 2c) showed that intense ion fluxes reached the upper limit of the FPI instrument. Thus, the incomplete measurement of ions would affect the calculation of the ion temperature and pressure and finally leave a great uncertainty to confirm whether the total pressure across the current layer is or is not balanced. However, the

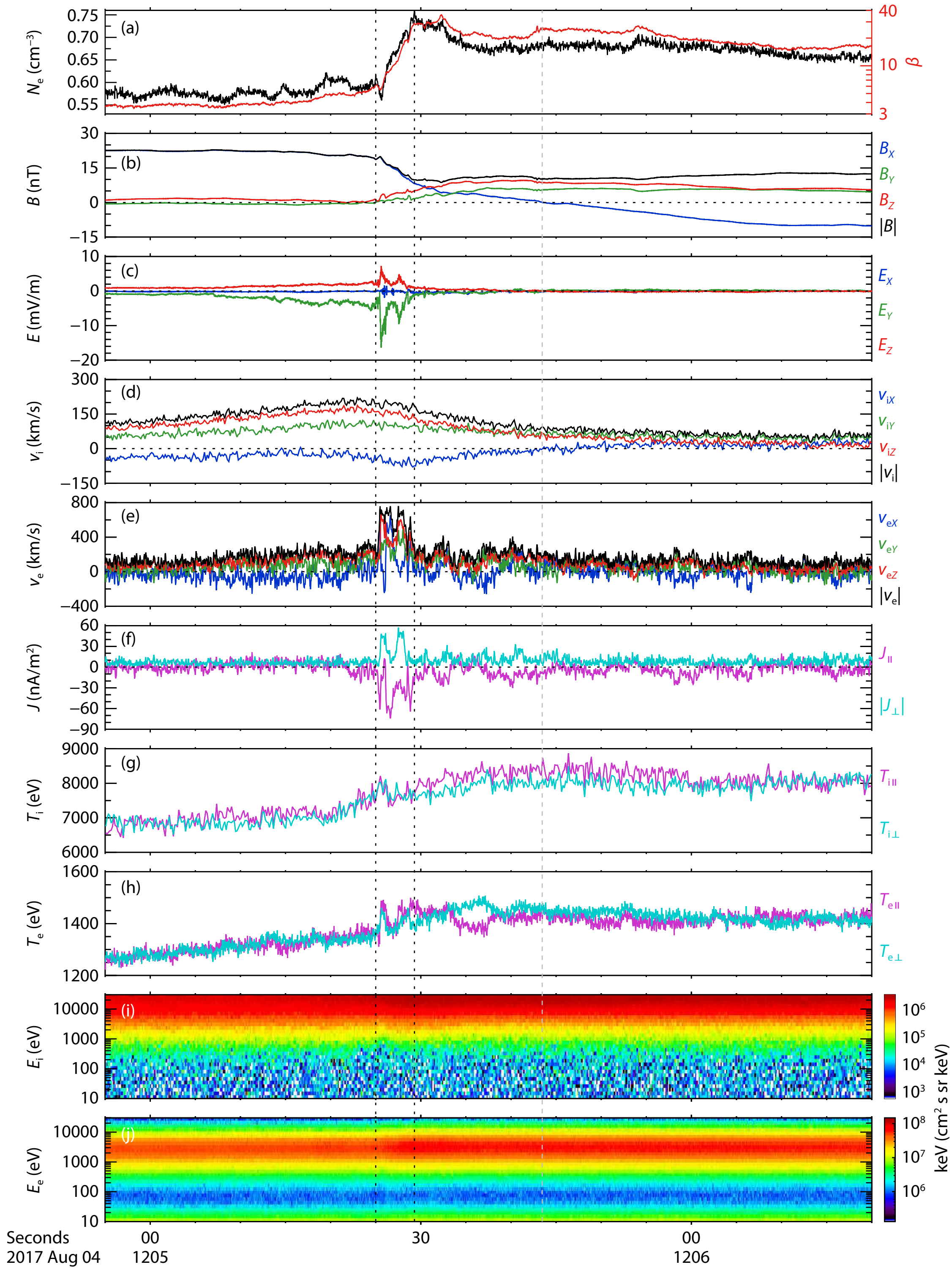

Figure 1. An overview of the asymmetric current layer crossing in the GSE coordinate system at the barycenter of four MMS satellites. (a) Electron number density N_e (black) and plasma β (red); (b) three components and magnitude of the magnetic field $\boldsymbol{B}$; (c) three components of the electric field $\boldsymbol{E}$; (d, e) three components and magnitude of the ion and electron bulk flow velocity $\boldsymbol{v}_i$, $\boldsymbol{v}_e$; (f) parallel and perpendicular components of current density $\boldsymbol{J} = qN(\boldsymbol{v}_i - \boldsymbol{v}_e)$; (g, h) ion and electron temperatures T_i, T_e parallel and perpendicular to the local magnetic field; (i, j) ion and electron differential energy flux E_i, E_e from the MMS1. The two vertical dotted lines (black) represent the time interval when the MMS observed the strong current layer, and the vertical dashed line (gray) represents the center of the plasma sheet.

FEEPS and EIS showed that the flux of high-energy ions after 12:05:29.4 UT was more intense than before 12:05:25 UT (Figures 2b and 2e). Thus, they both demonstrated ion pressure enhancements from before to after the current layer crossing, which indicated that the pressure imbalance was likely more than that calculated from the FPI measurements. This result further supports the

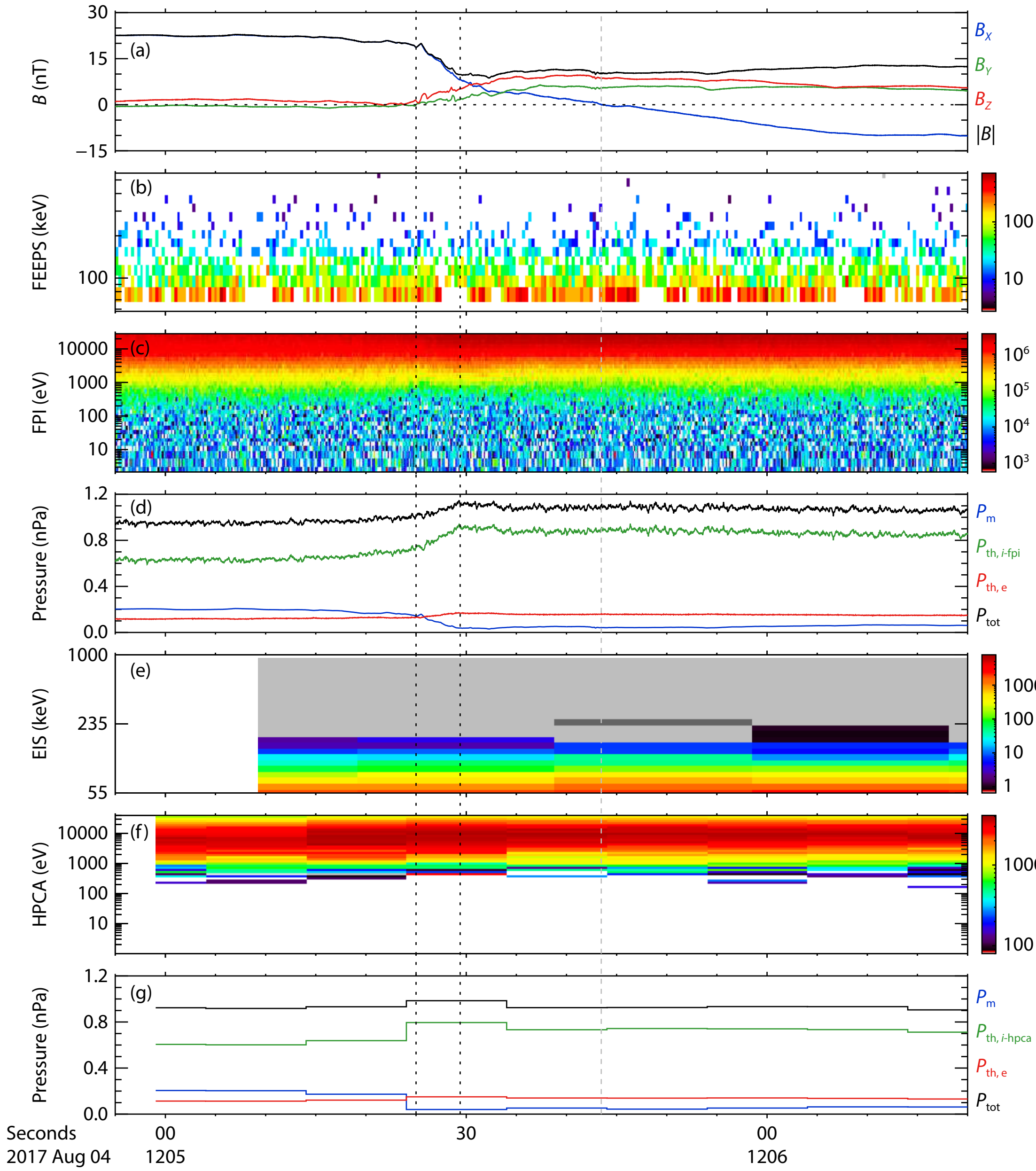

Figure 2. (a) Magnetic field $\boldsymbol{B}$; (b) high-energy ion flux measured by the FEEPS; (c) ion flux measured by the FPI; (d) magnetic pressure $P_m = B^2/2\mu_0$, ion pressure $P_{th,\,i\text{-fpi}} = N_e T_i$ with T_i from the FPI, electron pressure $P_{th,\,e} = N_e T_e$, and total pressure $P_{tot} = P_m + P_{th,\,i\text{-fpi}} + P_{th,\,e}$; (e) high-energy proton flux measured by the EIS; (f) proton flux measured by the HPCA; (g) magnetic pressure, proton pressure (with T_i from the HPCA), electron pressure, and total pressure.

pressure imbalance across the current layer. The HPCA showed that the ion flux and thermal pressure decreased after the current sheet crossing (Figures 2f and 2g), which likely occurred because energized ions lay in higher energies (in the FEEPS and EIS range) so that the pressure calculated from the HPCA energy range became low. Therefore, ion measurements from multiple instruments with different energy ranges suggested that the pressure was unbalanced across the current layer.

When the minimum directional derivative (MDD) method (Shi QQ et al., 2005) was applied, the average normal direction of the current layer from 12:05:25 to 12:05:29.4 UT was [0.033, 0.910, −0.413] in GSE coordinates, lying in the Y–Z plane, and the average normal velocity was 68.2 km/s from the spatiotemporal difference (STD) method (Shi QQ et al., 2006). Thus, its half-thickness along the normal direction was ~0.6 d_i, where d_i = 262.9 km was the ion inertial length based on N = 0.75 cm^{-3}. The result of the timing method (Schwartz, 1998) was consistent with those of the MDD and STD methods. In brief, the MMS observed an asymmetric sub-ion-scale current layer embedded at the edge of the magnetotail plasma sheet. The current layer was highly tilted and almost perpendicular to the equatorial plane, consistent with previous observations of the electron-scale current sheet (Wang RS et al., 2018).

Figure 3 shows the plasma parameter distribution across the

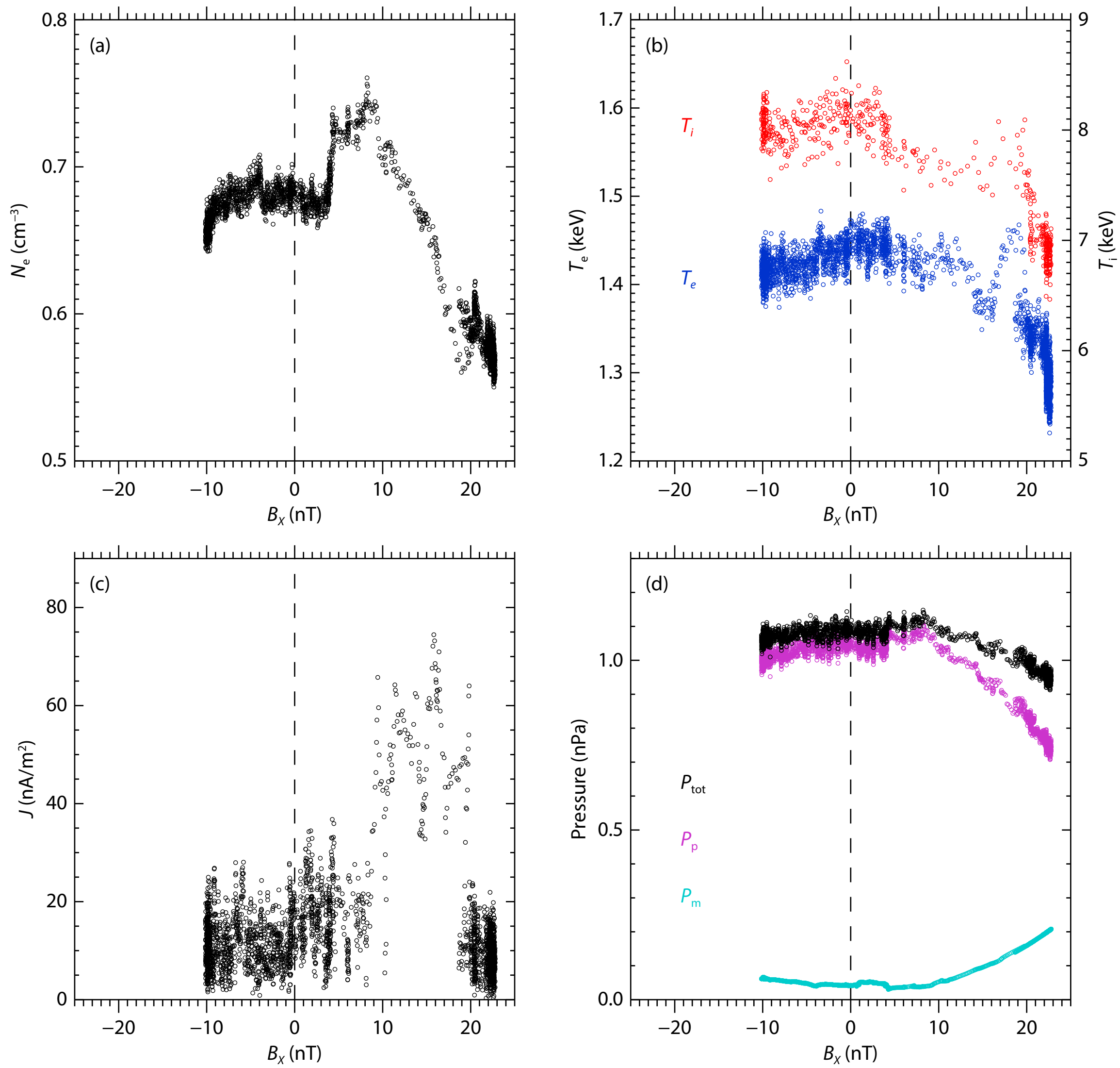

Figure 3. (a) Electron number density N_e; (b) ion and electron temperatures T_i, T_e; (c) total current density J; and (d) plasma pressure P_p, magnetic pressure P_m, and total pressure P_{tot} versus B_X during the crossing.

plasma sheet. Obviously, the plasma density peaked at around $B_X = 10$ nT instead of $B_X = 0$ nT (Figure 3a). The background plasma temperature, however, still maximized at around $B_X = 0$ nT (Figure 3b). The current density distribution clearly revealed that the embedded current layer existed only on the north edge of the plasma sheet (between $B_X = 9$ nT and $B_X = 19$ nT in Figure 3c). A strong gradient of plasma density existed across the current layer (between $B_X = 9$ nT and $B_X = 19$ nT in Figure 3a) and the ion and electron temperatures showed a local peak at around $B_X = 19$ nT (Figure 3b). As shown in Figure 1, the ion temperature began to be enhanced at ~12:05:20 UT, and the enhancement ended temporally at ~12:05:26 UT (Figure 1g), inconsistent with the duration of the current layer (12:05:25–12:05:29.4 UT). Thus, the enhancement of the ion temperature may not be associated with the current layer. The electron perpendicular temperature $T_{e\perp}$ peaked twice in the current layer, whereas the variation in the electron parallel temperature $T_{e\parallel}$ was more complicated (Figure 1h). What caused the variation in ion and electron temperatures across the current layer may still require further investigation.

Figure 3d shows the pressure distribution across the plasma sheet. It is obvious that the total pressure was basically balanced within the center of the plasma sheet by the magnetic pressure and the plasma pressure (between $B_X = -10$ nT and $B_X = 10$ nT), but it seemed to decrease gradually from $B_X \sim 9$ nT to $B_X \sim 19$ nT where the current layer was detected (i.e., the total pressure was unbalanced inside the current layer). The normal direction of the local plasma sheet at $B_X = 0$ nT given by the timing method was [−0.016, 0.995, −0.097] in GSE coordinates, which was mainly consistent with the normal direction of the current layer. A sketch map of the crossing of the current layer and the plasma sheet is shown in Figure 4.

2.2 An Embedded Current Layer Without a Magnetic Reconnection Signature

To further analyze the embedded asymmetric current layer, the observations were transferred into the local current coordinate system (*LMN*), as shown in Figure 5. Here, *N* was the average normal direction of the current layer from the MDD method, *M* =

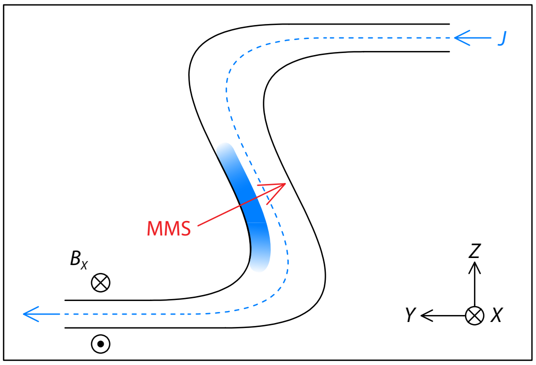

Figure 4. A sketch map of the crossing of the asymmetric current layer in the Y–Z plane in GSE coordinates. The region between the two solid black lines represents the magnetotail plasma sheet. The blue dashed line represents the center of the plasma sheet, and the blue region is the observed strong current layer. The red arrow represents the trajectory of the MMS.

$N \times L_{\text{MVA}-B}$ where $L_{\text{MVA}-B}$ is the maximum direction of the minimum variance analysis (MVA) of the magnetic field (Sonnerup and Scheible, 1998) from 12:05:24 to 12:05:30 UT, and $L = M \times N$ completed a right-handed orthogonal coordinate system. The resulting coordinates were L = [0.902, −0.206, −0.380], M = [−0.431, −0.360, −0.828], and N = [0.033, 0.910, −0.413] relative to the GSE coordinates. The magnetic field B_L was positive and pointed earthward in Figure 5a because the current layer was asymmetric and located in the northern hemisphere. The guide field B_M was strong and nearly constant (~−10 nT) during the crossing of the current layer. The parallel electron velocity $v_{e||}$ was basically positive except at ~12:05:26 UT (i.e., the electrons moved earthward along the magnetic field). The electron pitch angle distribution at the energies from 2 to 30 keV is shown in Figure 5j. The electron fluxes in the parallel direction (~0°–60°) were basically higher than those in the antiparallel direction (~120°–180°), which were slightly lower at ~12:05:26 UT. The variation in the electron pitch angle distribution supported the variation in $v_{e||}$, as shown in Figure 5c. Besides the field-aligned motion, the perpendicular velocity of electrons $|v_{e\perp}|$ was up to 700 km/s within the current layer (Figure 5c). The unipolar electric field was dominated by negative E_N (Figure 5d), and because the current layer was on the northern edge of the plasma sheet, the unipolar electric field E_N was directed toward the center of the plasma sheet. The unipolar electric field peaked during the interval when the perpendicular velocity $|v_{e\perp}|$ was enhanced. Figures 5e–5g show comparisons of the three components of the electric drift velocity $\boldsymbol{v}_{\boldsymbol{E}\times\boldsymbol{B}} = \boldsymbol{E} \times \boldsymbol{B}/B^2$, the perpendicular velocity of ions $\boldsymbol{v}_{i\perp}$, and the perpendicular velocity of electrons $\boldsymbol{v}_{e\perp}$, with the error from $\boldsymbol{E}$, $\boldsymbol{v}_i$, and $\boldsymbol{v}_e$. The perpendicular velocity of ions $\boldsymbol{v}_{i\perp}$ clearly deviated from $\boldsymbol{v}_{\boldsymbol{E}\times\boldsymbol{B}}$ in the L and M directions (Figures 5e and 5f), whereas $\boldsymbol{v}_{e\perp}$ was basically in agreement with $\boldsymbol{v}_{\boldsymbol{E}\times\boldsymbol{B}}$ in the L and M directions except for some local areas. In the normal direction, $v_{i\perp N}$ was approximately equal to zero and $v_{E\times B,N}$ showed little variation around zero. The disturbance of $v_{e\perp N}$ was obvious but mainly within the error of $v_{E\times B,N}$ except for some local regions. Because the electron bulk velocity had been manually preprocessed to reduce disturbance, we could not determine whether the local difference between $\boldsymbol{v}_{e\perp}$ and $\boldsymbol{v}_{\boldsymbol{E}\times\boldsymbol{B}}$ was from the measurement and processing of data or not. Nonetheless, we prefer to interpret the local difference as measurement error because their values were comparable. Accordingly, ions were demagnetized while electrons were still frozen to the magnetic field basically within the current layer. The separation of electrons and ions gave rise to the Hall electric field E_N relative to the background value. On the basis of the analysis above, we concluded that the magnetized electrons experienced electric field ($\boldsymbol{E} \times \boldsymbol{B}$) drift within the current layer, resulting in the formation of the intense electron current in the perpendicular direction, which was similar to the formation of an electron current in other magnetotail thin current sheets (Lu S et al., 2016, 2019; Wang RS et al., 2018).

The magnitude of the Hall electric field E_N was up to ~17 mV/m within the embedded current layer, which was significantly stronger than the typical value in the quiet current sheet (e.g., Lu S et al., 2019) but comparable to those in the reconnecting current sheets (e.g., Torbert et al., 2018; Zhou M et al., 2019b; Wang RS et al., 2020). During the interval, J_L was observed to reverse several times (Figure 5b), and B_M showed corresponding variations compared with the background value (~−9 nT; Figure 5a). Thus, the Hall current and Hall magnetic field were present in the current layer as well. The presence of the Hall electric field is normal because of the decoupling of ions and electrons in the sub-ion-scale current layer, unrelated to reconnection. On the other hand, a complicated Hall current and Hall magnetic field may not necessarily be associated with the occurrence of magnetic reconnection either. Therefore, the presence of the Hall electric field, Hall current, and Hall magnetic field may not be evidence of the occurrence of magnetic reconnection inside the sub-ion-scale current layer. Figure 5h shows the energy dissipation $\boldsymbol{J} \cdot (\boldsymbol{E} + \boldsymbol{v}_e \times \boldsymbol{B})$, with its error from $\boldsymbol{v}_i$, $\boldsymbol{v}_e$, and $\boldsymbol{E}$. As analyzed above, the disturbance of electron velocity led to the local difference between $\boldsymbol{v}_{e\perp}$ and $\boldsymbol{v}_{\boldsymbol{E}\times\boldsymbol{B}}$, which consequently resulted in the nonzero calculated energy dissipation. Because we interpreted this difference as measurement error, the suspicious nonzero $\boldsymbol{J} \cdot (\boldsymbol{E} + \boldsymbol{v}_e \times \boldsymbol{B})$ may not be real energy dissipation between the magnetic field and plasmas but from measurement error as well. Figure 5i shows the pseudo-agyrotropy of the electron velocity distribution functions from the MMS2 in the plane perpendicular to the magnetic field (see the detailed description by Li XM et al., 2019). The pseudo-agyrotropy values of the high-, medium-, and low-energy electrons were all equal to 1 approximately when the satellite passed through the current layer, indicating that the electrons were gyrotropic in the perpendicular plane throughout the time interval. The magnetized electrons, the absence of the nongyrotropic electron distribution and negligible energy dissipation from error, indicate that magnetic reconnection had not been triggered within the current layer.

Swisdak et al. (2003) proposed that the occurrence of magnetic reconnection depends on both the plasma β on the two sides of the current sheet and the magnetic shear angle θ across the current sheet. Additionally, Swisdak et al. (2010) predicted that magnetic reconnection is suppressed or enabled when the following relation is either satisfied or not satisfied:

$$\Delta\beta > 2\,(L/d_i)\tan(\theta/2),$$

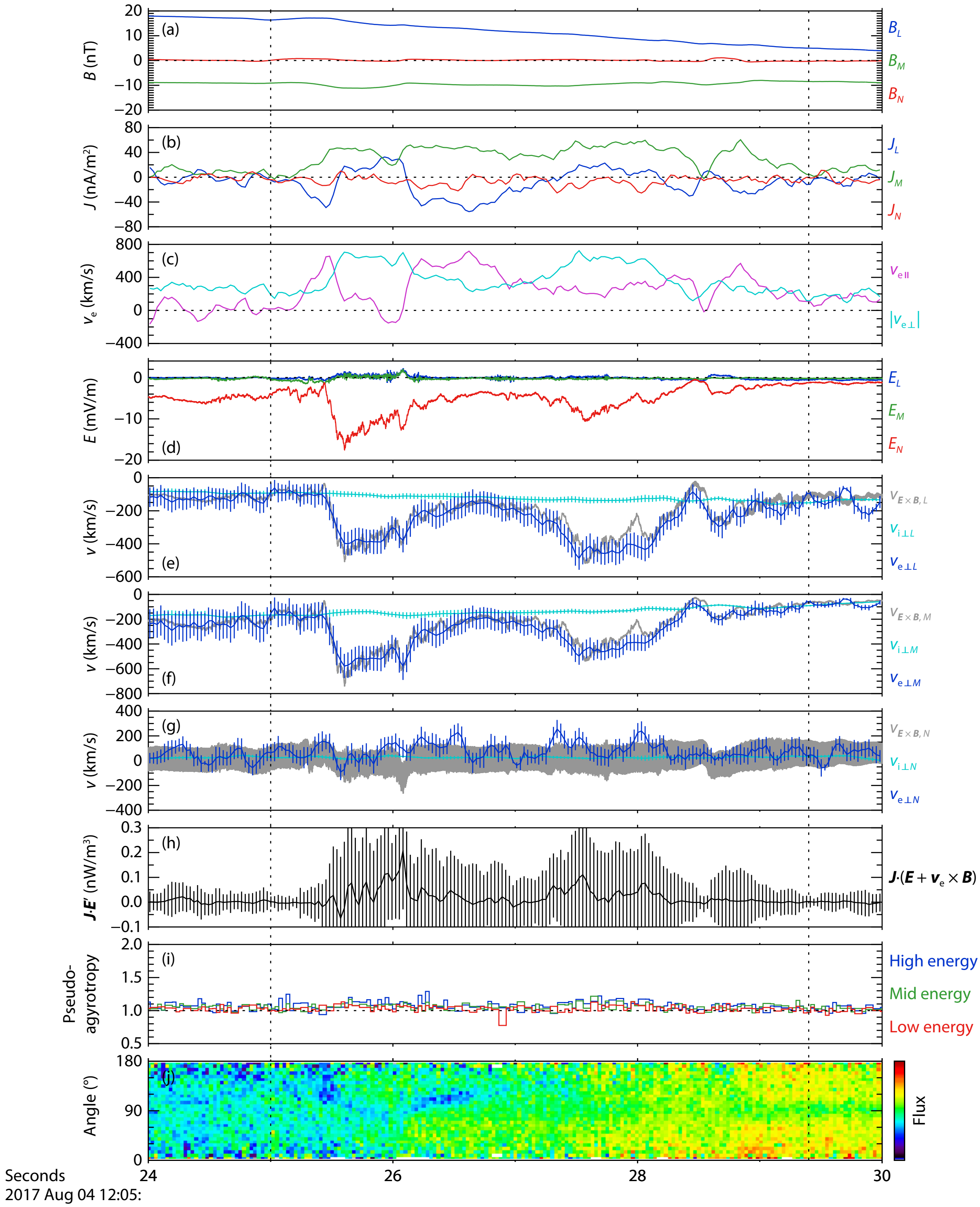

Figure 5. Observation of the current layer in the local current coordinate system (*LMN*). (a, b) Three components of the magnetic field $\boldsymbol{B}$ and current density $\boldsymbol{J}$; (c) parallel $\boldsymbol{v}_{e\|}$ and perpendicular $\boldsymbol{v}_{e\perp}$ electron bulk velocity; (d) three components of the electric field $\boldsymbol{E}$; (e–g) three components of $\boldsymbol{v}_{E\times B}$, $\boldsymbol{v}_{i\perp}$, and $\boldsymbol{v}_{e\perp}$, with the error from $\boldsymbol{E}$, $\boldsymbol{v}_i$, and $\boldsymbol{v}_e$; (h) energy dissipation $\boldsymbol{J}\cdot(\boldsymbol{E}+\boldsymbol{v}_e\times\boldsymbol{B})$, with the error from $\boldsymbol{E}$, $\boldsymbol{v}_i$, and $\boldsymbol{v}_e$; (i) the pseudo-agyrotropy of different energy segments in the perpendicular plane from the MMS2: high energy (3×10^4 to 4×10^4 km/s), medium energy (2×10^4 to 3×10^4 km/s), and low energy (0.5×10^4 to 2×10^4 km/s); (j) electron pitch angle distribution at the energies from 2 to 30 keV from the MMS2. The two vertical dotted lines represent the same time interval as in Figure 1.

where L is the current sheet thickness and d_i is the ion inertial length. This relation has been tested and proved to be universal by observations of the solar wind and magnetopause (Phan et al., 2010, 2013). The $\Delta\beta$ on the left side of the inequation represents the asymmetry of the plasma across the current sheet, and the magnetic shear angle θ on the right side reflects the influence of the guide field. In the case of symmetric reconnection, $\Delta\beta$ is close to zero and the relation is not satisfied until $\Delta\beta$ is small enough, that is, when magnetic reconnection is enabled in the symmetric current sheet in most cases and would be suppressed when the guide field is strong enough. With the increase in $\Delta\beta$, magnetic reconnection would be enabled in the case of large $\Delta\beta$ (i.e., a small guide field). For the asymmetric electron current layer observed in this event, $\Delta\beta$ was 20.4 ± 11.9 across the current layer, and the magnetic shear angle was 96° ± 49°. Thus, the relatively small magnetic shear angle but highly asymmetric plasma on the two sides of the current layer suppressed asymmetric reconnection in the current layer, as marked in Figure 6.

3. Conclusions and Discussion

In this work, we observed an asymmetric sub-ion-scale electron current layer embedded at the edge of the plasma sheet in the Earth's magnetotail, with a half-thickness of ~0.6 d_i. The current layer was highly tilted in the *Y*–*Z* plane, and electrons were the main current carriers inside. The ions were demagnetized, but the electrons were still frozen to the magnetic field line in the electron current layer. The decoupling of ions and electrons resulted in the Hall electric field, and the corresponding electric field drift of electrons led to the formation of the thin electron current layer. The magnetized electrons, the absence of the nongyrotropic electron distribution and negligible energy dissipation in the layer indicated that magnetic reconnection had not been triggered within it. The highly asymmetric plasma on the two sides of the current layer and low magnetic shear across it could have suppressed magnetic reconnection.

The Hall effect plays an important role in the current sheet when its thickness is comparable with the ion kinetic scale (Ma ZW and Bhattacharjee, 1998; Deng XH and Matsumoto, 2001; Øieroset et al., 2001). In this event, ions were decoupled from the magnetic field within the asymmetric current layer while electrons were still frozen to the magnetic field line. Therefore, the Hall electric field directed to the center of the plasma sheet was produced in the current layer. The magnetized electrons experienced electric field

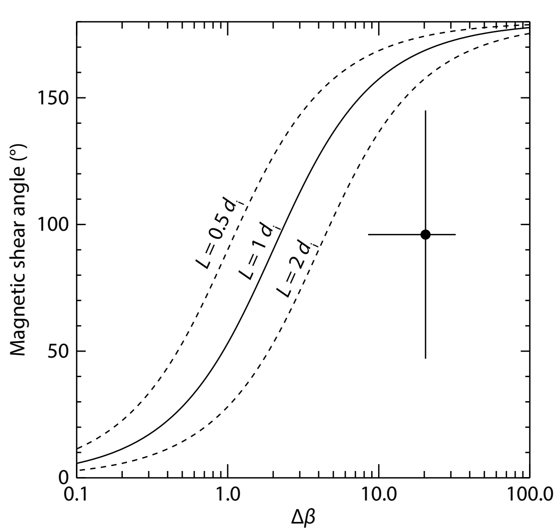

Figure 6. The average and full range of the magnetic shear angle versus $\Delta\beta$ across the electron current layer during the crossing.

($\boldsymbol{E} \times \boldsymbol{B}$) drift, resulting in the formation of current density in the perpendicular direction, which is similar to the mechanism of formation of other magnetotail thin current sheets (e.g., Lu S et al., 2016, 2019; Wang RS et al., 2018). The observed Hall electric field usually has a bipolar structure across the magnetotail current sheet directed toward the center of the current sheet, whereas it was unipolar in the asymmetric current layer in this event but directed to the center of the plasma sheet as well. Furthermore, although magnetic reconnection did not occur in this asymmetric current layer, the Hall electric field (~17 mV/m) and current density (~70 nA/m^2) inside were much more intense than those in the quiet-time magnetotail thin current sheet studied by Lu S et al. (2019), in which the typical magnitude of the Hall electric field was several tenths of 1 mV/m and the current density was ~10 nA/m^2. Furthermore, the guide field was strong (~−10 nT) in this asymmetric current layer (Figure 5a), whereas the crossing events with strong guide fields were excluded in the statistics by Lu S et al. (2019).

The Hall electric field has also been detected in reconnecting current sheets (e.g., Torbert et al., 2018; Wang RS et al., 2018; Li XM et al., 2019; Zhou M et al., 2019b). The magnitude of the Hall electric field is dominated by $\boldsymbol{J} \times \boldsymbol{B}$. In this event, the perpendicular current density $|J_\perp|$ was ~50 nA/m^2 in the current layer (Figure 1f), and the magnitude of the magnetic field was 10–20 nT (Figure 1b), both comparable to those in the reconnecting current sheets. Therefore, the magnitude of the Hall electric field in the current layer in this event was comparable to those in the reconnecting current sheets. Furthermore, the thickness of the Hall electric field was sub-ion scale in this event because the Hall electric field was associated with the perpendicular current component of the sub-ion-scale current layer. This scenario is slightly different from those in electron-scale reconnecting current sheets (e.g., Torbert et al., 2018), in which the thickness of the Hall electric field is electron scale. On the other hand, some reconnecting current sheets can be ion scale as well (e.g., Zhou M et al., 2019b), and the corresponding thickness of the Hall electric field can be ion scale.

One distinct feature of the embedded current layer is that an intense field-aligned electron bulk flow was found within it. This result is not unusual because the guide field was strong and constant (~−10 nT in Figure 5a). Some researchers may consider that the embedded current layer could be explained as a separatrix region away from the X-line in asymmetric magnetic reconnection. In the separatrix region, the electrons are usually observed to flow in and out along the magnetic field line (Nagai et al., 2001; André et al., 2004; Retinò et al., 2006; Lindstedt et al., 2009; Wang RS et al., 2013, 2014; Yu XC et al., 2019), so the electron bulk flows are commonly parallel or antiparallel to the magnetic field. In addition, perpendicular currents can exist on the separatrix (e.g., Zhong ZH et al., 2020). In this event, the parallel and perpendicular components of the electron current were basically equivalent in the current layer, so the current component might not be sufficient to confirm whether or not the current layer was a separatrix. On the other hand, the ion outflow was shifted toward the side with the stronger magnetic field in asymmetric reconnection (e.g., Pritchett and Mozer, 2009; Zhong ZH et al., 2022). Although the enhancement of the ion flow indeed appeared in the stronger magnetic field side (Figure 1d), the continuous and well-structural D-shaped ion velocity distribution functions did not appear to correspond to an enhancement of the ion flow, which is commonly associated with ion outflow (e.g., Eriksson et al., 2021). Thus, the enhancement of the ion flow in Figure 1d may not be related to the ion outflow. Another typical feature of the separatrix is the density cavity (e.g. Shay et al., 2001; Mozer et al., 2002; Wang RS et al., 2012, 2013; Zhong ZH et al., 2020). In this event, although the density showed a reduction temporally at ~12:05:26 UT (Figure 1a), the duration of the density reduction did not match the duration of the crossing of the current layer. Hence, the variation in density might not support the view that the current layer is a separatrix.

It is generally accepted that the magnetic field and the plasma are usually identical in both tail lobes so that symmetric magnetic reconnection will occur at the center of the magnetotail current sheet. However, the embedded current layer was asymmetric in this event. The plasma density (Figure 1a) below the current layer (after 12:05:29.4 UT, marked by the second dotted line in Figure 1) was higher than that above the layer (before 12:05:25 UT, marked by the first dotted line in Figure 1). Furthermore, the density peaked at ~12:05:30 UT, just between the high-density region and the low-density region. This variation in density could indicate that density compression occurred there. The normal direction of the local plasma sheet was mainly along the *Y* direction, and the embedded current layer was highly tilted in the *Y*–*Z* plane. The local deformation of the plasma sheet could be associated with the density compression, and it could have been beneficial for the formation of such a tilted embedded current layer at the edge of the plasma sheet.

Two parameters are used in Figure 7 to show the global environment of the 18 h around this event. The first parameter is the north–south component of the interplanetary magnetic field (IMF). When the IMF changes from northward to southward, it will begin to reconnect with the dayside northward geomagnetic field, which opens the Earth's magnetosphere and leads to strong global convection. As shown in Figure 7a, the IMF changed from northward to southward at ~06:30 UT and remained southward until ~15:30 UT. The second parameter is the auroral electrojet (*AE*) index, which represents the intensity of activity in the geomagnetic field. Figure 7b shows that the *AE* index began to increase gradually just when the IMF changed from northward to southward, and it then became enhanced abruptly from ~200 to ~1100 nT at ~8:00 UT, which is a typical signature of the growth and expansion phases of a magnetospheric substorm. However, just before the MMS observed the embedded asymmetric current layer without magnetic reconnection signatures, a substantial drop occurred in the IMF B_Z amplitude and the *AE* index decreased back to ~200 nT, which suggests that the substorm was interrupted at that time. The embedded asymmetric current layer might be a particular state of the magnetotail current sheet during the interruption of the ongoing substorm. The change in global environment might be conducive to local deformation and compression of the plasma sheet, and the suppression of magnetic reconnection in the current layer might contribute to the temporal interruption of the ongoing substorm. Nevertheless, it is difficult to prove causality rigorously between the local observation of the asymmetric current layer and the change in the global context. Thus, the formation of the embedded current layer and the role it plays still require further investigation.

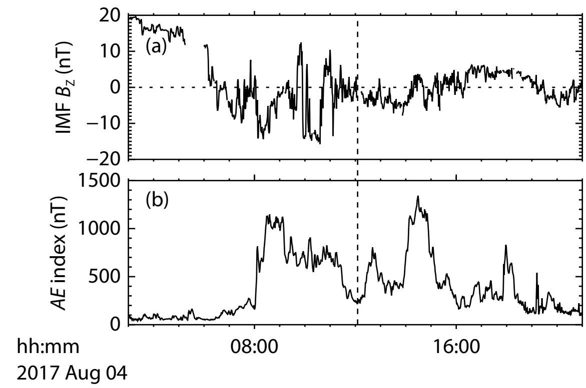

Figure 7. Global context of this event. (a) OMNI *Z* component of the IMF in the geocentric solar magnetospheric (GSM) coordinate system; (b) *AE* index. The vertical dashed line represents the time (12:05 UT) when the MMS observed the asymmetric electron current layer in the magnetotail.

Acknowledgments

This research was funded by the National Natural Science Foundation of China (NSFC, Grant No. 42174181) and the Key Research Program of Frontier Sciences, CAS (Grant No. QYZDJ-SSW-DQC010). All the MMS data used in this work are available at the MMS data center (https://lasp.colorado.edu/mms/sdc/). The data were loaded, analyzed, and plotted using Space Physics Environment Data Analysis Software (SPEDAS, Version 4.1; Angelopoulos et al., 2019), which is available at the site https://spedas.org/. The OMNI data are publicly available from CDAWeb (https://cdaweb.gsfc.nasa.gov/), and the *AE* index data are available on the website at http://wdc.kugi.kyoto-u.ac.jp/ae_provisional/.

References

André, M., Vaivads, A., Buchert, S. C., Fazakerley, A. N., and Lahiff, A. (2004). Thin electron-scale layers at the magnetopause. *Geophys. Res. Lett.*, *31*(3), L03803. https://doi.org/10.1029/2003GL018137

Angelopoulos, V., Cruce, P., Drozdov, A., Grimes, E. W., Hatzigeorgiu, N., King, D. A., Larson, D., Lewis, J. W., McTiernan, J. M., … Schroeder, P. (2019). The Space Physics Environment Data Analysis System (SPEDAS). *Space Sci. Rev.*, *215*(1), 9. https://doi.org/10.1007/s11214-018-0576-4

Asano, Y., Mukai, T., Hoshino, M., Saito, Y., Hayakawa, H., and Nagai, T. (2003). Evolution of the thin current sheet in a substorm observed by Geotail. *J. Geophys. Res.: Space Phys.*, *108*(A5), 1189. https://doi.org/10.1029/2002JA009785

Asano, Y., Mukai, T., Hoshino, M., Saito, Y., Hayakawa, H., and Nagai, T. (2004). Current sheet structure around the near-Earth neutral line observed by Geotail. *J. Geophys. Res.: Space Phys.*, *109*(A2), A02212. https://doi.org/10.1029/2003JA010114

Asano, Y., Nakamura, R., Baumjohann, W., Runov, A., Vörös, Z., Volwerk, M., Zhang, T. L., Balogh, A., Klecker, B., and Rème, H. (2005). How typical are atypical current sheets?. *Geophys. Res. Lett.*, *32*(3), L03108. https://doi.org/10.1029/2004GL021834

Baker, D. N., Pulkkinen, T. I., Angelopoulos, V., Baumjohann, W., and McPherron, R. L. (1996). Neutral line model of substorms: Past results and present view. *J. Geophys. Res.: Space Phys.*, *101*(A6), 12975–13010. https://doi.org/10.1029/

95JA03753

Baumjohann, W. (2002). Modes of convection in the magnetotail. *Phys. Plasmas*, *9*(9), 3665–3667. https://doi.org/10.1063/1.1499116

Baumjohann, W., Roux, A., Le Contel, O., Nakamura, R., Birn, J., Hoshino, M., Lui, A. T. Y., Owen, C. J., Sauvaud, J. A., … Runov, A. (2007). Dynamics of thin current sheets: Cluster observations. *Ann. Geophys.*, *25*(6), 1365–1389. https://doi.org/10.5194/angeo-25-1365-2007

Blake, J. B., Mauk, B. H., Baker, D. N., Carranza, P., Clemmons, J. H., Craft, J., Crain, W. R. Jr., Crew, A., Dotan, Y., … Westlake, J. (2016). The Fly's Eye Energetic Particle Spectrometer (FEEPS) sensors for the magnetospheric multiscale (MMS) mission. *Space Sci. Rev.*, *199*(1-4), 309–329. https://doi.org/10.1007/s11214-015-0163-x

Burch, J. L., Moore, T. E., Torbert, R. B., and Giles, B. L. (2016). Magnetospheric multiscale overview and science objectives. *Space Sci. Rev.*, *199*(1-4), 5–21. https://doi.org/10.1007/s11214-015-0164-9

Deng, X. H., and Matsumoto, H. (2001). Rapid magnetic reconnection in the Earth's magnetosphere mediated by whistler waves. *Nature*, *410*(6828), 557–560. https://doi.org/10.1038/35069018

Ergun, R. E., Tucker, S., Westfall, J., Goodrich, K. A., Malaspina, D. M., Summers, D., Wallace, J., Karlsson, M., Mack, J., … Cully, C. M. (2016). The axial double probe and fields signal processing for the MMS mission. *Space Sci. Rev.*, *199*(1-4), 167–188. https://doi.org/10.1007/s11214-014-0115-x

Eriksson, S., Ma, X. Y., Burch, J. L., Otto, A., Elkington, S., and Delamere, P. A. (2021). MMS observations of double mid-latitude reconnection ion beams in the early non-linear phase of the Kelvin–Helmholtz instability. *Front. Astron. Space Sci.*, *8*, 760885. https://doi.org/10.3389/fspas.2021.760885

Genestreti, K. J., Farrugia, C. J., Lu, S., Vines, S. K., Reiff, P. H., Phan, T., Baker, D. N., Leonard, T. W., Burch, J. L., … Turner, D. L. (2023). Multi-scale observation of magnetotail reconnection onset: 2. Microscopic dynamics. *J. Geophys. Res.: Space Phys.*, *128*(11), e2023JA031760. https://doi.org/10.1029/2023JA031760

Harris, E. G. (1962). On a plasma sheath separating regions of oppositely directed magnetic field. *Nuovo Cimento*, *23*(1), 115–121. https://doi.org/10.1007/BF02733547

Li, X. M., Wang, R. S., Lu, Q. M., Hwang, K. J., Zong, Q. G., Russell, C. T., and Wang, S. (2019). Observation of nongyrotropic electron distribution across the electron diffusion region in the magnetotail reconnection. *Geophys. Res. Lett.*, *46*(24), 14263–14273. https://doi.org/10.1029/2019GL085014

Lindqvist, P. A., Olsson, G., Torbert, R. B., King, B., Granoff, M., Rau, D., Needell, G., Turco, S., Dors, I., … Tucker, S. (2016). The spin-plane double probe electric field instrument for MMS. *Space Sci. Rev.*, *199*(1-4), 137–165. https://doi.org/10.1007/s11214-014-0116-9

Lindstedt, T., Khotyaintsev, Y. V., Vaivads, A., André, M., Fear, R. C., Lavraud, B., Haaland, S., and Owen, C. J. (2009). Separatrix regions of magnetic reconnection at the magnetopause. *Ann. Geophys.*, *27*(10), 4039–4056. https://doi.org/10.5194/angeo-27-4039-2009

Lu, S., Lin, Y., Angelopoulos, V., Artemyev, A. V., Pritchett, P. L., Lu, Q. M., and Wang, X. Y. (2016). Hall effect control of magnetotail dawn–dusk asymmetry: A three-dimensional global hybrid simulation. *J. Geophys. Res.: Space Phys.*, *121*(12), 11882–11895. https://doi.org/10.1002/2016JA023325

Lu, S., Artemyev, A. V., Angelopoulos, V., Lin, Y., Zhang, X. J., Liu, J., Avanov, L. A., Giles, B. L., Russell, C. T., and Strangeway, R. J. (2019). The Hall electric field in Earth's magnetotail thin current sheet. *J. Geophys. Res.: Space Phys.*, *124*(2), 1052–1062. https://doi.org/10.1029/2018JA026202

Lu, S., Wang, R. S., Lu, Q. M., Angelopoulos, V., Nakamura, R., Artemyev, A. V., Pritchett, P. L., Liu, T. Z., Zhang, X. J., … Wang, S. (2020). Magnetotail reconnection onset caused by electron kinetics with a strong external driver. *Nat. Commun.*, *11*(1), 5049. https://doi.org/10.1038/s41467-020-18787-w

Ma, Z. W., and Bhattacharjee, A. (1998). Sudden enhancement and partial disruption of thin current sheets in the magnetotail due to Hall MHD effects. *Geophys. Res. Lett.*, *25*(17), 3277–3280. https://doi.org/10.1029/98GL02432

Mauk, B. H., Blake, J. B., Baker, D. N., Clemmons, J. H., Reeves, G. D., Spence, H. E., Jaskulek, S. E., Schlemm, C. E., Brown, L. E., … Westlake, J. H. (2016). The Energetic Particle Detector (EPD) investigation and the energetic ion spectrometer (EIS) for the Magnetospheric Multiscale (MMS) mission. *Space Sci. Rev.*, *199*(1-4), 471–514. https://doi.org/10.1007/s11214-014-0055-5

Mozer, F. S., Bale, S. D., and Phan, T. D. (2002). Evidence of diffusion regions at a subsolar magnetopause crossing. *Phys. Rev. Lett.*, *89*(1), 015002. https://doi.org/10.1103/PhysRevLett.89.015002

Nagai, T., Shinohara, I., Fujimoto, M., Hoshino, M., Saito, Y., Machida, S., and Mukai, T. (2001). Geotail observations of the Hall current system: Evidence of magnetic reconnection in the magnetotail. *J. Geophys. Res.: Space Phys.*, *106*(A11), 25929–25949. https://doi.org/10.1029/2001JA900038

Nakamura, R., Baumjohann, W., Runov, A., and Asano, Y. (2006). Thin current sheets in the magnetotail observed by Cluster. *Space Sci. Rev.*, *122*(1-4), 29–38. https://doi.org/10.1007/s11214-006-6219-1

Ness, N. F. (1965). The Earth's magnetic tail. *J. Geophys. Res.*, *70*(13), 2989–3005. https://doi.org/10.1029/JZ070i013p02989

Øieroset, M., Phan, T. D., Fujimoto, M., Lin, R. P., and Lepping, R. P. (2001). *In situ* detection of collisionless reconnection in the Earth's magnetotail. *Nature*, *412*(6845), 414–417. https://doi.org/10.1038/35086520

Petrukovich, A. A., Artemyev, A. V., Malova, H. V., Popov, V. Y., Nakamura, R., and Zelenyi, L. M. (2011). Embedded current sheets in the Earth's magnetotail. *J. Geophys. Res.: Space Phys.*, *116*(A5), A00I25. https://doi.org/10.1029/2010JA015749

Phan, T. D., Gosling, J. T., Paschmann, G., Pasma, C., Drake, J. F., Øieroset, M., Larson, D., Lin, R. P., and Davis, M. S. (2010). The dependence of magnetic reconnection on plasma β and magnetic shear: Evidence from solar wind observations. *Astrophys. J.*, *719*(2), L199–L203. https://doi.org/10.1088/2041-8205/719/2/L199

Phan, T. D., Paschmann, G., Gosling, J. T., Oieroset, M., Fujimoto, M., Drake, J. F., and Angelopoulos, V. (2013). The dependence of magnetic reconnection on plasma *β* and magnetic shear: Evidence from magnetopause observations. *Geophys. Res. Lett.*, *40*(1), 11–16. https://doi.org/10.1029/2012GL054528

Pollock, C., Moore, T., Jacques, A., Burch, J., Gliese, U., Saito, Y., Omoto, T., Avanov, L., Barrie, A., … Zeuch, M. (2016). Fast plasma investigation for magnetospheric multiscale. *Space Sci. Rev.*, *199*(1-4), 331–406. https://doi.org/10.1007/s11214-016-0245-4

Pritchett, P. L., and Mozer, F. S. (2009). Asymmetric magnetic reconnection in the presence of a guide field. *J. Geophys. Res.: Space Phys.*, *114*(A11), A11210. https://doi.org/10.1029/2009JA014343

Retinò, A., Vaivads, A., André, M., Sahraoui, F., Khotyaintsev, Y., Pickett, J. S., Bavassano Cattaneo, M. B., Marcucci, M. F., Morooka, M., … Cornilleau-Wehrlin, N. (2006). Structure of the separatrix region close to a magnetic reconnection X-line: Cluster observations. *Geophys. Res. Lett.*, *33*(6), L06101. https://doi.org/10.1029/2005GL024650

Runov, A., Nakamura, R., Baumjohann, W., Zhang, T. L., Volwerk, M., Eichelberger, H. U., and Balogh, A. (2003). Cluster observation of a bifurcated current sheet. *Geophys. Res. Lett.*, *30*(2), 1036. https://doi.org/10.1029/2002GL016136

Runov, A., Sergeev, V. A., Baumjohann, W., Nakamura, R., Apatenkov, S., Asano, Y., Volwerk, M., Vörös, Z., Zhang, T. L., … Rème, H. (2005). Electric current and magnetic field geometry in flapping magnetotail current sheets. *Ann. Geophys.*, *23*(4), 1391–1403. https://doi.org/10.5194/angeo-23-1391-2005

Runov, A., Sergeev, V. A., Nakamura, R., Baumjohann, W., Apatenkov, S., Asano, Y., Takada, T., Volwerk, M., Vörös, Z., … Balogh, A. (2006). Local structure of the magnetotail current sheet: 2001 Cluster observations. *Ann. Geophys.*, *24*(1), 247–262. https://doi.org/10.5194/angeo-24-247-2006

Russell, C. T., and McPherron, R. L. (1973). The magnetotail and substorms. *Space Sci. Rev., 15*(2–3). https://doi.org/10.1007/BF00169321

Russell, C. T., Anderson, B. J., Baumjohann, W., Bromund, K. R., Dearborn, D., Fischer, D., Le, G., Leinweber, H. K., Leneman, D., … Richter, I. (2016). The Magnetospheric multiscale magnetometers. *Space Sci. Rev.*, *199*(1-4), 189–256. https://doi.org/10.1007/s11214-014-0057-3

Schwartz, S. J. (1998). Shock and discontinuity normals, Mach numbers, and related parameters. In G. Paschmann, et al. (Eds.), *Analysis Methods for Multi-Spacecraft Data*. Noordwijk, Netherlands: The International Space Science Institute.

Sergeev, V., Runov, A., Baumjohann, W., Nakamura, R., Zhang, T. L., Volwerk, M., Balogh, A., Rème, H., Sauvaud, J. A., … Klecker, B. (2003). Current sheet flapping motion and structure observed by Cluster. *Geophys. Res. Lett.*, *30*(6), 1327. https://doi.org/10.1029/2002GL016500

Sergeev, V., Runov, A., Baumjohann, W., Nakamura, R., Zhang, T. L., Balogh, A., Louarnd, P., Sauvaud, J. A., and Reme, H. (2004). Orientation and propagation of current sheet oscillations. *Geophys. Res. Lett.*, *31*(5), L05807. https://doi.org/10.1029/2003GL019346

Shay, M. A., Drake, J. F., Rogers, B. N., and Denton, R. E. (2001). Alfvénic collisionless magnetic reconnection and the Hall term. *J. Geophys. Res.: Space Phys.*, *106*(A3), 3759–3772. https://doi.org/10.1029/1999JA001007

Shen, C., Liu, Z. X., Li, X., Dunlop, M., Lucek, E., Rong, Z. J., Chen, Z. Q., Escoubet, C. P., Malova, H. V., … Mouikis, C. (2008a). Flattened current sheet and its evolution in substorms. *J. Geophys. Res.: Space Phys.*, *113*(A7), A07S21. https://doi.org/10.1029/2007JA012812

Shen, C., Rong, Z. J., Li, X., Dunlop, M., Liu, Z. X., Malova, H. V., Lucek, E., and Carr, C. (2008b). Magnetic configurations of the tilted current sheets in magnetotail. *Ann. Geophys.*, *26*(11), 3525–3543. https://doi.org/10.5194/angeo-26-3525-2008

Shi, Q. Q., Shen, C., Pu, Z. Y., Dunlop, M. W., Zong, Q. G., Zhang, H., Xiao, C. J., Liu, Z. X., and Balogh, A. (2005). Dimensional analysis of observed structures using multipoint magnetic field measurements: Application to Cluster. *Geophys. Res. Lett.*, *32*(12), L12105. https://doi.org/10.1029/2005GL022454

Shi, Q. Q., Shen, C., Dunlop, M. W., Pu, Z. Y., Zong, Q. G., Liu, Z. X., Lucek, E., and Balogh, A. (2006). Motion of observed structures calculated from multi-point magnetic field measurements: Application to Cluster. *Geophys. Res. Lett.*, *33*(8), L08109. https://doi.org/10.1029/2005GL025073

Sitnov, M. I., Stephens, G. K., Tsyganenko, N. A., Miyashita, Y., Merkin, V. G., Motoba, T., Ohtani, S., and Genestreti, K. J. (2019). Signatures of nonideal plasma evolution during substorms obtained by mining multimission magnetometer data. *J. Geophys. Res.: Space Phys.*, *124*(11), 8427–8456. https://doi.org/10.1029/2019JA027037

Sonnerup, B. U. Ö., and Scheible, M. (1998). Minimum and maximum variance analysis. In G. Paschmann and P. W. Daly (Eds.), *Analysis Methods for Multi-Spacecraft Data* (pp. 185–220). Bern, Switzerland: European Space Agency.

Swisdak, M., Rogers, B. N., Drake, J. F., and Shay, M. A. (2003). Diamagnetic suppression of component magnetic reconnection at the magnetopause. *J. Geophys. Res.: Space Phys.*, *108*(A5), 1218. https://doi.org/10.1029/2002JA009726

Swisdak, M., Opher, M., Drake, J. F., and Alouani Bibi, F. (2010). The vector direction of the interstellar magnetic field outside the heliosphere. *Astrophys. J.*, *710*(2), 1769–1775. https://doi.org/10.1088/0004-637X/710/2/1769

Torbert, R. B., Burch, J. L., Phan, T. D., Hesse, M., Argall, M. R., Shuster, J., Ergun, R. E., Alm, L., Nakamura, R., … Saito, Y. (2018). Electron-scale dynamics of the diffusion region during symmetric magnetic reconnection in space. *Science*, *362*(6421), 1391–1395. https://doi.org/10.1126/science.aat2998

Wang, R. S., Nakamura, R., Lu, Q. M., Du, A. M., Zhang, T. L., Baumjohann, W., Khotyaintsev, Y. V., Volwerk, M., André, M., … Lu, S. (2012). Asymmetry in the current sheet and secondary magnetic flux ropes during guide field magnetic reconnection. *J. Geophys. Res.: Space Phys.*, *117*(A7), A07223. https://doi.org/10.1029/2011JA017384

Wang, R. S., Du, A. M., Nakamura, R., Lu, Q. M., Khotyaintsev, Y. V., Volwerk, M., Zhang, T. L., Kronberg, E. A., Daly, P. W., Fazakerley, A. N. (2013). Observation of multiple sub-cavities adjacent to single separatrix. *Geophys. Res. Lett.*, *40*(11), 2511–2517. https://doi.org/10.1002/grl.50537

Wang, R. S., Lu, Q. M., Khotyaintsev, Y. V., Volwerk, M., Du, A. M., Nakamura, R., Gonzalez, W. D., Sun, X., Baumjohann, W., … Wu, M. Y. (2014). Observation of double layer in the separatrix region during magnetic reconnection. *Geophys. Res. Lett.*, *41*(14), 4851–4858. https://doi.org/10.1002/2014GL061157

Wang, R. S., Lu, Q. M., Nakamura, R., Baumjohann, W., Huang, C., Russell, C. T., Burch, J. L., Pollock, C. J., Gershman, D., … Giles, B. (2018). An electron-scale current sheet without bursty reconnection signatures observed in the near-Earth tail. *Geophys. Res. Lett.*, *45*(10), 4542–4549. https://doi.org/10.1002/2017GL076330

Wang, R. S., Lu, Q. M., Lu, S., Russell, C. T., Burch, J. L., Gershman, D. J., Gonzalez, W., and Wang, S. (2020). Physical implication of two types of reconnection electron diffusion regions with and without ion-coupling in the magnetotail current sheet. *Geophys. Res. Lett.*, *47*(21), e2020GL088761. https://doi.org/10.1029/2020GL088761

Young, D. T., Burch, J. L., Gomez, R. G., De Los Santos, A., Miller, G. P., Wilson IV, P., Paschalidis, N., Fuselier, S. A., Pickens, K., … Webster, J. M. (2016). Hot plasma composition analyzer for the magnetospheric multiscale mission. *Space Sci. Rev.*, *199*(1-4), 407–470. https://doi.org/10.1007/s11214-014-0119-6

Yu, X. C., Wang, R. S., Lu, Q. M., Russell, C. T., and Wang, S. (2019). Nonideal electric field observed in the separatrix region of a magnetotail reconnection event. *Geophys. Res. Lett.*, *46*(19), 10744–10753. https://doi.org/10.1029/2019GL082538

Zhang, T. L., Baumjohann, W., Nakamura, R., Balogh, A., and Glassmeier, K. H. (2002). A wavy twisted neutral sheet observed by CLUSTER. *Geophys. Res. Lett.*, *29*(19), 1899. https://doi.org/10.1029/2002GL015544

Zhong, Z. H., Tang, R. X., Zhou, M., Deng, X. H., Pang, Y., Paterson, W. R., Giles, B. L., Burch, J. L., and Tobert, R. B. (2018). Evidence for secondary flux rope generated by the electron Kelvin–Helmholtz instability in a magnetic reconnection diffusion region. *Phys. Rev. Lett.*, *120*(7), 075101. https://doi.org/10.1103/PhysRevLett.120.075101

Zhong, Z. H., Zhou, M., Tang, R. X., Deng, X. H., Khotyaintsev, Y. V., Giles, B. L., Paterson, W. R., Pang, Y., Man, H. Y., and Burch, J. L. (2020). Extension of the electron diffusion region in a guide field magnetic reconnection at magnetopause. *Astrophys. J.*, *892*(1), L5. https://doi.org/10.3847/2041-8213/ab7b7c

Zhong, Z. H., Zhou, M., Liu, Y. H., Deng, X. H., Tang, R. X., Graham, D. B., Song, L. J., Man, H. Y., Pang, Y., and Khotyaintsev, Y. V. (2022). Stacked electron diffusion regions and electron Kelvin–Helmholtz vortices within the ion diffusion region of collisionless magnetic reconnection. *Astrophys. J. Lett.*, *926*(2), L27. https://doi.org/10.3847/2041-8213/ac4dee

Zhou, M., Huang, J., Man, H. Y., Deng, X. H., Zhong, Z. H., Russell, C. T., Paterson, W. R., Giles, B. L., Lindqvist, P. A., … Burch, J. L. (2019a). Electron-scale vertical current sheets in a bursty bulk flow in the terrestrial magnetotail. *Astrophys. J. Lett.*, *872*(2), L26. https://doi.org/10.3847/2041-8213/ab0424

Zhou, M., Deng, X. H., Zhong, Z. H., Pang, Y., Tang, R. X., El-Alaoui, M., Walker, R. J., Russell, C. T., Lapenta, G., … Lindqvist, P. A. (2019b). Observations of an electron diffusion region in symmetric reconnection with weak guide field. *Astrophys. J.*, *870*(1), 34. https://doi.org/10.3847/1538-4357/aaf16f

Zhou, M., Man, H. Y., Deng, X. H., Pang, Y., Khotyaintsev, Y., Lapenta, G., Yi, Y. Y., Zhong, Z. H., and Ma, W. Q. (2021). Observations of secondary magnetic reconnection in the turbulent reconnection outflow. *Geophys. Res. Lett.*, *48*(4), e2020GL091215. https://doi.org/10.1029/2020GL091215